JOURNAL OF Materials CHEMISTRY

Synthesis, structure and electrochemistry of $LiMn_{2-y}Al_yO_4$ prepared by a wet-chemistry method

C. Julien,* S. Ziolkiewicz, M. Lemal and M. Massot

Laboratoire des Milieux Désordonnés et Hétérogènes, UMR 7603 Université Pierre et Marie Curie, 4 place Jussieu, case 86, 75252 Paris cedex 05, France. E-mail: cjul@ccr.jussieu.fr

Received 2nd January 2001, Accepted 1st May 2001
First published as an Advance Article on the web 6th June 2001

The $LiMn_{2-y}Al_yO_4$ spinel phases have been synthesised by wet-chemistry techniques using a methanolic solution of the metal acetates and dicarboxylic acid as a complexing agent. The formation temperature of $LiMn_{2-y}Al_yO_4$ powders has been found to be as low as 350 °C using the succinic acid method. The physical properties of the synthesised products have been investigated by X-ray diffraction, Raman spectroscopy, thermal analyses, and electrical conductivity. To improve the rechargeable capacity of Li//$LiMn_2O_4$ cells, the electrochemical performances of $LiMn_{2-y}Al_yO_4$ compounds as positive electrodes have been evaluated. The structural properties of the materials are very similar to $LiMn_2O_4$, the electrochemical performances show that the capacity is maintained at 95% of the initial value at the 50th cycle, this being explained by the change of the Mn^{3+}/Mn^{4+} ratio in doped phases.

1. Introduction

Among the insertion compounds used in rechargeable lithium-ion batteries, the $LiMn_2O_4$ spinel phase is an attractive positive electrode material due to its low cost and high environmental acceptability. Its use in rechargeable lithium-ion cells stems from the fact that the Li^+ ions can be removed and reinserted into this compound topotactically.[1–5] Reversible insertion–extraction occurs in the 4 V range and gives rise to two voltage plateaux at 4.05 and 4.15 V *vs.* Li/Li^+. Instead, its moderate specific gravimetric capacity of 148 mA h g^{-1} tends to decline upon cycling. This behaviour has been connected to such factors as (i) slow dissolution of the material as a consequence of a disproportionation reaction, (ii) relative structural instability when the limit λ-MnO_2 (spinel structure) is approached at the end of charge, and (iii) the Jahn–Teller effect at the end of discharge when the Mn^{3+}/Mn^{4+} ratio is higher than unity.[6]

In recent years, several investigations have been made to overcome capacity fading by doping with several cations.[6–11] Lowering of the Mn^{3+} concentration has been achieved by substitution of monovalent, divalent or trivalent ions for Mn ions in $LiMn_{2-y}M_yO_4$ spinels (M = Al, Co, Mg, Cr, Ni, Fe, Ti and Zn). Gummow *et al.*[6] have pointed out that doping with Li^+ or Mg^{2+} enhances the stability of the $LiMn_2O_4$ spinel phase. Le Cras *et al.*[12] have evaluated the recyclability of $LiMn_{1.5}Mg_{0.5}O_4$ below 3 V. Guohua *et al.*[13] have suggested that the improvement of the stability is due to stronger M–O bonding of the MO_6 octahedron of partially substituted $LiMn_{2-y}M_yO_4$ (M = Co, Cr, Ni) in comparison with that in the parent $LiMn_2O_4$ spinel. The lithium intercalation properties of $LiAlMnO_4$ have been reported by Le Cras *et al.*,[12] while $LiMn_{2-y}Al_yO_4$ compounds grown by solid-state reaction have been studied by Song *et al.*[9]

In this context, we have synthesised $LiMn_{2-y}Al_yO_4$ spinel phases by adopting the wet-chemistry approach, which provides good stoichiometric control of the electrochemically-active spinel materials. Obviously, the preparation of spinel $LiMn_2O_4$ by the low-temperature technique, referred to as *soft chemistry*, produces more homogeneous, pure, and more reproducible phases. The morphology and microstructure of the samples can be experimentally controlled in contrast to the conventional solid-state reaction products obtained at high temperature, which do not ensure a high level of homogeneity in the final composition. Recently, several low-temperature preparation techniques such as sol–gel,[14–15] precipitation,[16] Pechini process,[17] and hydrothermal synthesis[18] have been developed. Prabaharan *et al.*[19,20] have reported efficient low-temperature processes for the bulk preparation of spinel $LiMn_2O_4$ which exhibit the above features. Thackeray *et al.*[21] have studied the thermal stability of stoichiometric spinel phase $LiMn_2O_4$. They concluded that low synthesis temperatures ensure single phase products, while high synthesis temperatures, *ca.* 800 °C, diminish the structural stability of the spinel product. Considerable progress has been made by employing solution techniques in obtaining high-performance cathode-active materials.[22,23]

This paper presents the synthesis of spinel $LiMn_{2-y}Al_yO_4$ ($0.0 \leqslant y \leqslant 0.3$) by a wet chemistry method. The effect of partial Al^{3+} substitution for Mn^{3+} in $LiMn_2O_4$ positive electrodes on its electrochemical behaviour in Li cells has been investigated. Physical properties have been studied by X-ray diffraction (XRD), Raman scattering (RS) spectroscopy, differential and thermal analyses (DTA/TG), and electrical conductivity. The electrochemical activity of the synthesised $LiMn_{2-y}Al_yO_4$ has been tested in lithium-containing test cells that include the above spinels as positive electrodes by means of the galvanostatic (multiple charge–discharge) technique.

2. Experimental

Undoped $LiMn_2O_4$ and $LiMn_{2-y}Al_yO_4$ ($0.1 \leqslant y \leqslant 0.3$) powders were prepared with the same technique, *i.e.* the succinic acid-assisted wet chemistry technique. In this technique, the dicarboxylic acid ($C_4H_6O_4$, $M = 118.09$) plays the role of chelating agent. Stoichiometric proportions of high purity manganese, aluminium, and lithium acetates (AR-grade from Aldrich) are dissolved in a minimum volume of methanol or distilled water. An equal volume of a 1 mol l^{-1} aqueous solution of succinic acid is added as a complexing agent in the above methanolic or aqueous solution. The concentration of the complexing agent is adjusted carefully to get a solution with the pH in the range between 3–4. Upon adding the above

complexing agent, homogeneous precipitates are obtained owing to the poor solubility of manganese and lithium succinates, which are finely dispersed in the solution medium. It is believed that the carboxylic (COOH) groups on the succinic acid form a chemical bond with the metal ions and these mixtures develop the extremely viscous paste-like substance upon slow evaporation of methanol. It is also presumed that the lithium and transition metal cations are trapped homogeneously within the paste and ensure molecular level mixing. This eliminates the need for long-range diffusion during the subsequent formation of spinel lithium manganate.

The paste is further dried at 120 °C to obtain the dried precursor mass. The precursor is then allowed to decompose in air at around 300 °C. The decomposition results in a large exothermic reaction which originates from the combustion of organic species present in the precursor mass. This exothermic process enhances the oxidation reaction and onset of the phase formation of the spinel compound. The process yields a blue-black voluminous mass of spinel $LiMn_{2-y}Al_yO_4$. Experimental details regarding the access of oxygen to the reactants during the combustion stage, as well as specification of the time of heat treatment and oxidation, have been described in a previous paper.[23]

The structure of the $LiMn_{2-y}Al_yO_4$ samples was characterised by X-ray powder diffraction (XRPD) using a diffractometer (Philips model PW1830) with nickel-filtered CuKα radiation ($\lambda = 1.5406$ Å). The diffraction patterns were taken at room temperature in the range of $5° < 2\theta < 80°$ using step scans. The XRD data were analysed by the Rietveld profile refinements using the Fullprof program. The thermal decomposition behaviour of the gel precursors was examined by means of differential thermal analysis (DTA) using a Netzsch analyser (model STA 409). Experiments were carried out under ambient atmosphere with a heating rate of 0.1 °C s^{-1}. Raman scattering (RS) spectra were taken at room temperature in a quasi-backscattering configuration. A Jobin-Yvon (model U1000) double monochromator with holographic gratings and a computer-controlled photon-counting system was used. The laser light source was the 514.5 nm line radiation from a Spectra-Physics 2020 argon-ion laser. RS spectra are the average of 12 scans obtained with a spectral resolution of 2 cm^{-1}. To avoid sample photodecomposition or denaturation, RS spectra were recorded using a low excitation power of 10 mW. The d.c. electrical conductivity was measured using a two-terminal method. The test samples were prepared in the form of pellets of 0.5 mm thickness and 10 mm diameter by pressing at 150 MPa for 300 s under vacuum. The pellet was inserted between spring loaded nickel electrodes. Measurements were carried out in the temperature range 150–500 K using a one-zone furnace and a SMC-TBT cryostat. The temperature was kept constant to within $\pm$0.5–1 K.

Electrochemical studies were carried out on the synthesised product annealed at 550 °C in order to test its suitability as a positive electrode-active material in high voltage lithium-containing batteries. The above tests were performed to measure quantitatively the electrochemical capacity of the synthesised spinel product. The laboratory-scale Li//Li-$Mn_{2-y}Al_yO_4$ cells were housed in a Teflon laboratory-cell apparatus employing a non-aqueous Li^+ ion conducting organic electrolyte. The electrolyte was a 1 M $LiPF_6$ in EC–DMC in 1 : 1 volumetric ratio. A microporous polypropylene film (Celgard 2500) was used as a separator. A typical composite cathode consisted of a mixture of spinel $LiMn_{2-y}Al_yO_4$ powders (550 °C), acetylene black and colloidal PTFE binder in a 90 : 5 : 5 weight ratio. The PTFE–acetylene black was used to provide good electrical conductivity as well as mechanical toughness between active grains. To assess the quasi-open-circuit voltage profiles, galvanostatic charge–discharge cycles were recorded in slow scan mode using a Mac-Pile system as follows. A current density of 0.1 mA cm^{-2} was supplied for 1 h, corresponding to lithium extraction of about 0.01 mol from 1 mol of the electrode material. This was followed by a relaxation time of 0.5 h before the next charging started. The charging was stopped when the closed-circuit voltage reached 4.4 V. The apparent lithium content of the charge–discharge compounds was estimated using the current passed and the mass of the electrode material.

3. Results and discussion

3.1. Synthesis and structural characterisation

The exact temperature of the phase formation reaction of the spinel $LiMn_{2-y}Al_yO_4$ has been studied using thermogravimetric analysis (DTA/TG) on the precursor complex. Fig. 1 shows the thermogram of $LiMn_{1.9}Al_{0.1}O_4$ in the range from 30 to 600 °C. These results display two discrete weight-loss regions occurring at *ca.* 110 and 290 °C. The DTA curve shows two distinguishable transformation enthalpies. An endothermic peak observed at about 110 °C is accompanied by a noticeable weight loss in the TG curve. This is attributed to the superficial water loss due to the hygroscopic nature of the precursor complex. As the process of heating continues, an exothermic transformation begins to appear at 309 °C indicating the onset of the decomposition and/or the soft oxidation of the molecular precursor. The huge exothermic reaction indicates the decomposition of organic species present in the precursor complex, which burn in the presence of atmospheric oxygen. More than 30% of the weight loss occurring during this stage arises from the violent oxidation–decomposition reaction. It appears that succinic acid acts as a fuel in the pyrolysis of the molecular precursors and accelerates the process of decomposition as mentioned above. This process leads to the formation of the spinel structure when the precursor is heated at 350 °C.

The structure of the resulting $LiMn_{2-y}Al_yO_4$ products was investigated by XRPD as presented in Fig. 2. The results show well-defined peaks even at temperatures as low as 350 °C, indicating that the product obtained immediately after decomposition has gained the single-phase spinel structure without any residual impurities observable from XRPD measurements. XRPD diagrams exhibit patterns with the strongest (111) Bragg line. The Bragg peaks of the $LiMn_{2-y}Al_yO_4$ compounds measured after annealing the decomposed product at 550 °C were indexed to a cubic system with a lattice parameter which was refined with space group *Fd*3*m*. Unit cell parameters in the cubic setting were determined by the least squared method using thirteen diffraction lines. For the undoped $LiMn_2O_4$ material heated at 550 °C, we found $a = 8.2360 \pm 0.0017$ Å, in good agreement with the literature value for the spinel $LiMn_2O_4$.[8,16] The structures of $LiMn_{1-y}Al_yO_4$ ($y = 0.1$, 0.3) nominal composition materials were analysed by Rietveld refinement of their XRD patterns as

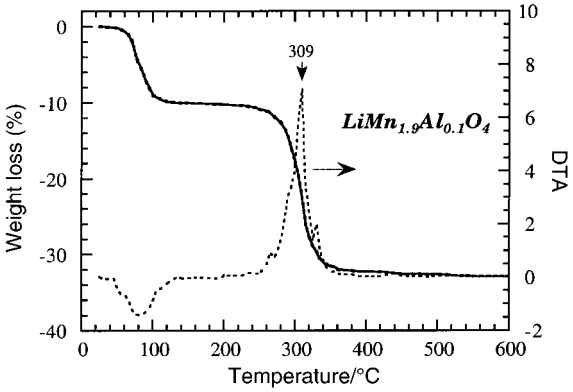

Fig. 1 Thermogravimetric curve of the precursor complex of $LiMn_{1.9}Al_{0.1}O_4$. Full line, TG; dashed line, DTA.

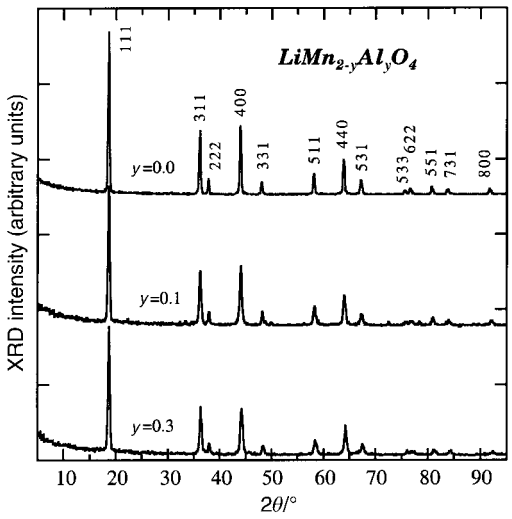

Fig. 2 Powder X-ray diffraction patterns of $LiMn_{2-y}Al_yO_4$ ($0.0 \leqslant y \leqslant 0.3$) samples annealed at 550 °C. Bragg lines are indexed using the cubic lattice with space group *Fd*3*m*.

shown in Table 1. These results show that $LiMn_{1-y}Al_yO_4$ samples exhibit patterns which are characteristic of the normal spinel structure (*Fd*3*m* space group) with an appropriate site occupancy for cations.

As compared with $LiMn_2O_4$, the lattice parameters of $LiMn_{2-y}Al_yO_4$ decreased with increasing substituted Al content. The (440) Bragg line and those in the interval $56° \leqslant 2\theta \leqslant 72°$ display a slight displacement due to the decrease of the lattice parameter. Fig. 3 shows the variation of the cubic lattice parameter of $LiMn_{2-y}Al_yO_4$ as a function of the Al content. It is obvious that slight lattice parameter shifts are observed, concordant with Mn^{3+} substitution by Al^{3+} and consistent with the results of previous workers.[9] It is a fact that Al forms with Mg^{2+} the $MgAl_2O_4$ phase with the normal spinel structure, in which the Al ions occupy the octahedral interstices. Indeed, several spinel compounds including $MgAl_2O_4$ are prone to inversion. Similar occupancy can be considered in the $LiMn_{2-y}Al_yO_4$ spinel. One can observe that Mn^{3+} has a radius of 0.64 Å and Al^{3+} has a radius of 0.54 Å for a coordination number of 6.[24] The former is a Jahn–Teller ion while the latter is not. Our XRPD structure profile refinement suggests that Al replaces Mn^{3+} in the 16d octahedral site, since we do not observe the appearance of a strong (220) Bragg line (at *ca.* $2\theta = 30°$), which is extremely sensitive to the occupancy of the 8a tetrahedral site.

3.2. Physical properties

The $LiMn_{2-y}Al_yO_4$ powders annealed at 550 °C were also characterised by means of vibrational spectroscopy to determine the local structure and the nature of the cationic environment in the spinel phase. Fig. 4 shows the room temperature RS spectrum of undoped $LiMn_2O_4$ and those of

Table 1 Refined crystallographic parameters for $LiMn_{2-y}Al_yO_4$ samples as determined from X-ray diffraction data[a]

y(Al)	Atom	Site	Position	*B*/Å^2	Site occupancy (%)
0.1	Li	8a	0.125	1.29	98
	Al	16d	0.5	0.41	11
	Mn	16d	0.5	0.44	89
	O	32e	0.263	0.95	100
0.3	Li	8a	0.125	2.30	97
	Al	16d	0.5	0.40	28
	Mn	16d	0.5	0.38	72
	O	32e	0.263	0.65	100

[a] $R_p = 6.9\%$, $R_{Bragg} = 5.4\%$.

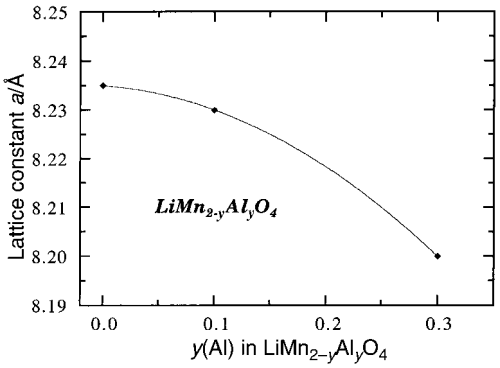

Fig. 3 Variation of the cubic lattice parameter of $LiMn_{2-y}Al_yO_4$ as a function of the Al content.

the synthesised $LiMn_{2-y}Al_yO_4$ samples annealed at 550 °C for $y = 0.1$ and $y = 0.3$ (curves a–c, respectively). As reported before,[25–27] the RS spectrum of $LiMn_2O_4$ is dominated by a strong and broad band at *ca.* 625 cm^{-1} with a shoulder at 580 cm^{-1}. A band with a medium intensity appears at *ca.* 482 cm^{-1}, while three weak bands are observed at *ca.* 370, 298 and 204 cm^{-1}. The RS spectra of $LiMn_{2-y}Al_yO_4$ powders are similar to their $LiMn_2O_4$ counterpart.

The cubic spinel possesses the O_h^7 spectroscopic symmetry. It has a general structural formula $Li[Mn_2]O_4$, where the manganese cations reside on the octahedral 16d sites, the oxygen anions on the 32e sites, and the lithium ions occupy

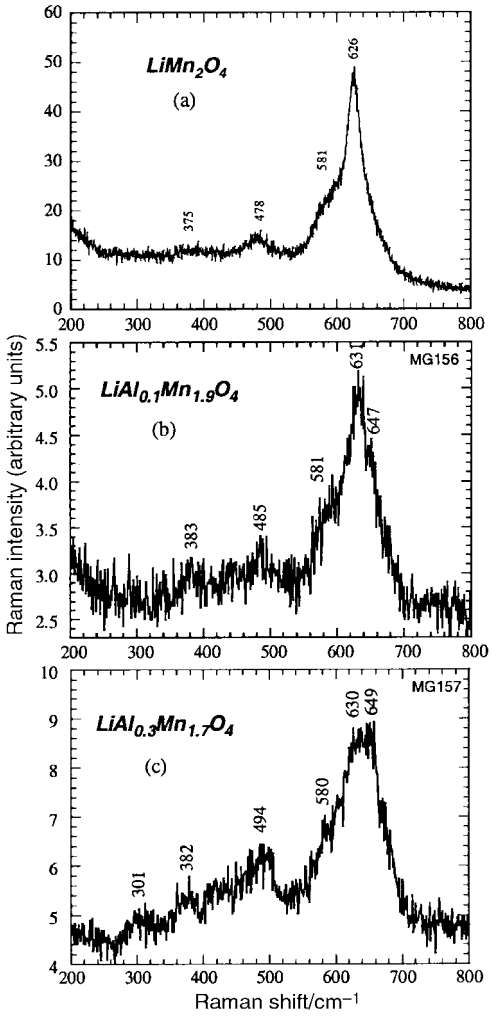

Fig. 4 Raman scattering spectra of samples $LiMn_{2-y}Al_yO_4$ (a) $y = 0.0$, (b) $y = 0.1$, and (c) $y = 0.3$ annealed at 550 °C. Spectra recorded with the 514.5 nm line of an Ar^+ laser line at 10 mW power excitation.

the tetrahedral 8a sites. Analysis of the vibrational spectra of $LiMn_2O_4$ with O_h^7 (*Fd3m* space group) yields nine optic modes.[28] Five modes are Raman active ($A_{1g}+E_g+3F_{2g}$) and four are infrared active (F_{1u}). It is also convenient to analyse these spectra in terms of localised vibrations, considering that the spinel structure is built of MnO_6 octahedra and LiO_4 tetrahedra.[25] For $LiMn_{1.9}Al_{0.1}O_4$, the Raman band located at *ca.* 631 cm^{-1} can be viewed as the symmetric Mn–O stretching vibration of MnO_6 groups. This band is assigned to A_{1g} symmetry in the O_h^7 spectroscopic space group. Its broadening is related to the cation–anion bond lengths and polyhedral distortion occurring in $LiMn_{2-y}Al_yO_4$. The intensity of the shoulder located at 580 cm^{-1} is slightly enhanced upon aluminium substitution. This may be due to the change of Mn^{3+} and Mn^{4+} proportions *vs.* Al in the material. The RS peaks located at 383 and 485 cm^{-1} have the F_{2g} symmetry. One can state that in the ideal cubic spinel $LiMn_2O_4$, the Mn^{3+} and Mn^{4+} cations are considered as crystallographically equivalent (16d sites) in agreement with XRD data. Then, occupation probabilities of 0.5 must be affected for each cation in 16d site. Hence, a loss of translation invariance certainly occurs in $LiMn_{2-y}Al_yO_4$, due to local lattice distortion around the different Mn^{3+} and Mn^{4+} cations. As a result, a breakdown in the Raman selection rules is expected, which explains the observation of broad bands (disorder) and the fact that more modes than expected are observed in cubic $LiMn_{1.7}Al_{0.3}O_4$ (Fig. 4c).

Fig. 5 displays the temperature dependence of the d.c. conductivity, σ_{dc}, of $LiMn_{2-y}Al_yO_4$ as a function of the aluminium composition in the spinel lattice. These Arrhenius plots of the electrical conductivity for $LiMn_{2-y}Al_yO_4$ show that over the compositional range $0.0 \leqslant y \leqslant 0.3$ the conduction is thermally activated owing to the semiconducting character of these oxides.[29] The electrical conductivity varies from 10^{-8} to 10^{-2} S cm^{-1} in the temperature range from 150 to 500 K. Examination of the data (Fig. 5) indicates that (i) the electrical conductivity is sensitive to the aluminium content in the host lattice, (ii) a noticeable change in the activation energy is observed in the low temperature region, (iii) the temperature dependence of σ_{dc} deviates markedly from the exponential law—a curvature appears in the Arrhenius plots—and (iv) the phase transition nearby ambient temperature disappears for Al-doped $LiMn_2O_4$. The room temperature electrical conductivity increases by one order of magnitude from 10^{-5} S cm^{-1} for $LiMn_2O_4$ to 10^{-4} S cm^{-1} for $LiMn_{1.7}Al_{0.3}O_4$.

According to the electronic considerations discussed by Goodenough *et al.*,[30] the small-polaron semiconducting character of the $Li[Mn^{3+}Mn^{4+}]O_4$ compound is due to weak Mn–Mn interactions, which prevents an itinerant-electron bandwidth giving localised electronic configurations. Considering

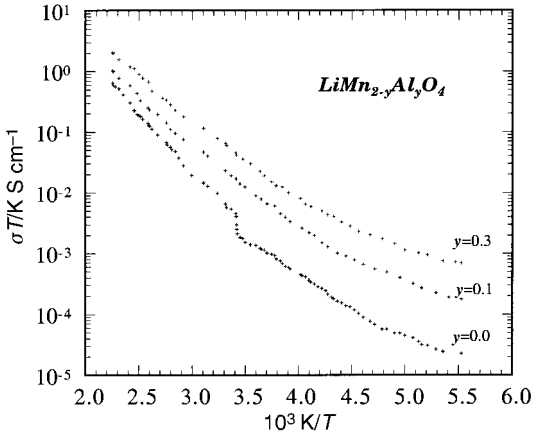

Fig. 5 Arrhenius plots of the electrical conductivity of $LiMn_{2-y}Al_yO_4$ ($0.0 \leqslant y \leqslant 0.3$) samples.

the model of small-polaron transport suggested by Austin and Mott,[31] the d.c. conductivity should be given by

$$\sigma_h = AC(1-C)T^{-1}\exp[-2\alpha R - W/k_BT] \quad (1)$$

where A is a constant, C the concentration of one type of cation, R the average interionic separation, α^{-1} the radius of the localised wavefunction (usually $\approx$10 Å in transition metal oxides), W the activation energy, T the absolute temperature and k_B the Boltzman constant. For the undoped $LiMn_2O_4$ spinel, the room temperature conductivity is *ca.* 10^{-5} S cm^{-1} and the activation energy is 0.161 eV. These values are typical of small-polaron conduction in a mixed-valent system. In fact, the $LiMn_2O_4$ material imposes equal quantities of Mn^{4+} and Mn^{3+} ions per formula unit, which allows for easy transfer of electrons *via* hopping. The Al substitution increases the average valency of the manganese ions from $Mn^{3.50+}$ for cubic structure $LiMn_2O_4$ to $Mn^{3.59+}$ for the $LiMn_{1.7}Al_{0.3}O_4$ phase. Thus the electrical conductivity of lithium manganese oxides with the spinel structure depends strongly on the valencies of the cations and their distribution among the crystallographic positions in the framework. Enhancement of the electrical conductivity originates from three factors: (1) the increase of carrier concentration due to the change in the average valency, (2) the decrease of the Mn–O distances in the structure which reduces the average interionic separation, and (3) the decrease of the activation energy due to the slight modification of the electronic band structure upon Al substitution. In addition, we observed the disappearance of the phase transition which occurs near room temperature in undoped $LiMn_2O_4$. This first-order phase transition has been attributed to a cooperative effect of the Jahn–Teller Mn^{3+} ions.[32,33] The distortion is suppressed by aluminium substitution due to an increase of the average Mn valency. A loss of translation invariance certainly occurs, due to local lattice distortions around the different Mn^{3+} and Mn^{4+} cations.

3.3. Electrochemical properties

The electrochemical features of synthesised spinel $LiMn_{2-y}Al_yO_4$ were examined using $Li//LiMn_{2-y}Al_yO_4$ cells subjected to constant current cycling. The results from the electrochemical $Li//LiMn_{2-y}Al_yO_4$ cell are presented as plots of cell voltage *vs.* capacity (Fig. 6a,b) as well as curves of the inverse derivative $-(\partial x/\partial V)$ *versus* capacity (Fig. 7a,b). Plateaux in voltage *versus* capacity give rise to peaks in $-(\partial x/\partial V)$; so derivative plots are useful for displaying details. Fig. 6a and b show the charge–discharge curves at the first cycle of $Li//LiMn_{2-y}Al_yO_4$ cells for $y=0.1$ and 0.3, respectively, under galvanostatic conditions at 22 °C. The cells were charged and discharged at current densities of 0.5 mA cm^{-2}, while the voltage is monitored between 3.0 and 4.4 V. In this potential domain, the charge–discharge curves correspond to the voltage profiles characteristic of the spinel $LiMn_2O_4$ cathode material associated with lithium occupancy of tetrahedral sites, in agreement with previous works.[3–9] From the variation of the cell potential for the complete cell (Fig. 6), one can see the presence of two regions during the lithium insertion–extraction processes. The shape of the voltage curves indicates whether the delithiated $LiMn_{2-y}Al_yO_4$ exists as a single or a multiple phase. In the latter case the potential is expected to be essentially invariant with composition. The first region (I) is characterised by an S-shaped voltage curve, whereas the second region (II) corresponds to a plateau portion. In region I, the charge voltage increases continuously in the voltage range of 3.80–4.05 V. In region II, the charge voltage is stable around 4.15 V. However, the phase diagram of $Li_xMn_2O_4$ compounds *vs.* lithium content is a current debate. Recent studies have shown that extraction/insertion reactions occur with five different domains induced by three cubic phases separated by two-phase regions.[34,35] From the results shown in Figs. 6 and 7, for region II corresponding

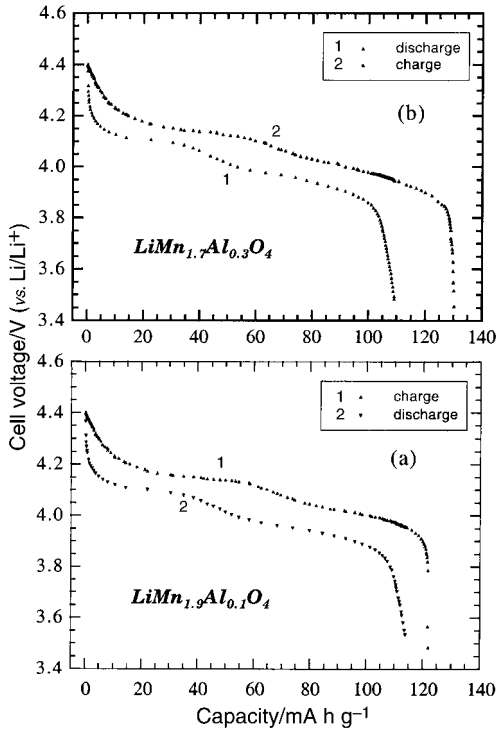

Fig. 6 Electrochemical features of Li//$LiMn_{2-y}Al_yO_4$ cells during the first charge–discharge cycle: (a) $y=0.1$ and (b) $y=0.3$. The non-aqueous cells employing the electrolyte of composition 1 M $LiPF_6$ in EC–DMC (1 : 1) were cycled in the voltage range 2.5–4.4 V at 0.5 mA cm^{-2} current density.

to the upper voltage plateau, a two-phase system is recognised, whereas the region I can be attributed to a single phase characterised by an S-shaped voltage curve. The two regimes of intercalation are clearly depicted when the derivative voltage $-(\partial x/\partial V)$ is plotted *vs.* cell voltage (Fig. 7). The broad band centered at 4.05 V (capacity around $x=0.7$) is indicative of the one-phase system, while the narrow band at 4.15 V (capacity around 0.4) is indicative of the two-phase system. For the Li//$LiMn_{1.7}Al_{0.3}O_4$ cell (Fig. 6b), the upper 4 V plateau provides over 109 mA h g^{-1} based on the active material utilisation with an excellent cyclability.

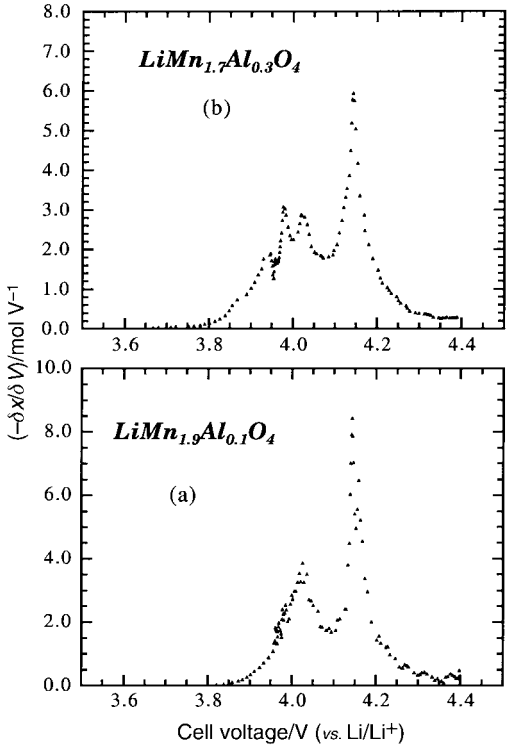

Fig. 7 Inverse derivative voltage $-(\partial x/\partial V)$ *versus* capacity of the first charge curve of the Li//$LiMn_{2-y}Al_yO_4$ cells: (a) $y=0.1$ and (b) $y=0.3$.

Fig. 8 shows the discharge capacity *versus* cycle number of Li//$LiMn_{2-y}Al_yO_4$ cells ($y=0.0$, 0.1, and 0.3). The products have been found to be excellent in terms of practical material utilisation capacity of 109 mA h g^{-1} for $LiMn_{1.7}Al_{0.3}O_4$. It is obvious that the initial capacity is decreased with increasing Al content. This is due to the decreasing amount of Mn^{3+} ions in the substituted spinel phase since during the intercalation–deintercalation of Li^+ in $LiMn_2O_4$ only the Mn^{3+} contributes to the charge capacity. Obviously, the Al incorporation improves the cyclability of the Li//$LiMn_{2-y}Al_yO_4$ cells. The substituted $LiMn_{2-y}Al_yO_4$ spinel phases are more stable than $LiMn_2O_4$, and the capacity fading is less for $y=0.3$ than for $y=0.1$. For $y=0.3$, the capacity of the Li//$LiMn_{1.7}Al_{0.3}O_4$ cell is maintained at 95% of the initial capacity at the 50th cycle.

The electrochemical stability has been attributed to the suppression of the Jahn–Teller distortion caused by Mn^{3+} ions and to the stronger metal–oxygen bonding in substituted $LiMn_{2-y}Al_yO_4$ spinel phases.[9] In a compound like $LiMn_{1.7}Al_{0.3}O_4$, Mn would have an average oxidation number of 3.59, corresponding to a $Mn^{3+}:Mn^{4+}$ ratio of 41 : 59, which would make ratios smaller than 1 more probable in the final discharge stage. In $LiMn_{1.9}Al_{0.1}O_4$, the Mn oxidation number is 3.53 which is close to the theoretical value for undoped spinel. This suggests that the electrochemical stability of this compound is less than that of the former as shown in Fig. 8.

4. Conclusion

We have synthesised $LiMn_{2-y}Al_yO_4$ spinel powders using a simple low-temperature wet-chemistry assisted process using a methanolic solution of metal acetates and dicarboxylic acid as a complexing agent. The formation temperature of $LiMn_{2-y}Al_yO_4$ spinel phases has been found to be as low as 350 °C using a succinic acid method. This procedure readily offers a single phase compound suitable for use as a positive electrode-active material for Li-ion batteries. The structural properties of the materials are very similar to $LiMn_2O_4$, a slight decrease of the cubic cell parameter is observed with increasing aluminium content.

The Al substitution in the spinel lattice induces an increase in the electrical conductivity. This evolution is due essentially to the degree of oxidation of manganese ions and a modification of the average Mn valency. This observation leads to the suggestion that the electronic energy band model for conductivity is the hopping of electrons between the two charge states of Mn^{3+} and Mn^{4+} ions. As a result, the phase transition close to room temperature disappears in $LiMn_{2-y}Al_yO_4$ samples due to the suppression of the distortion by

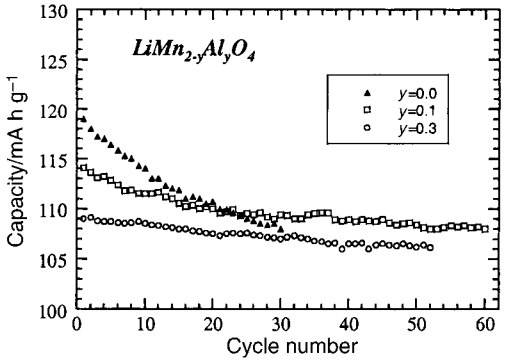

Fig. 8 Discharge capacity *versus* cycle number of Li//$LiMn_{2-y}Al_yO_4$ cells: (a) $y=0.0$, (b) $y=0.1$ and (c) $y=0.3$.

aluminium substitution, which induces an increase of the average Mn valency.

The products have been found to be excellent in terms of the practical material utilisation capacity of 109 mA h g^{-1} for $LiMn_{1.7}Al_{0.3}O_4$. The spinel $LiMn_{2-y}Al_yO_4$ powders have been proven to be electrochemically active when employed as the positive electrode in lithium rechargeable cells.

Acknowledgements

The authors wish to thank Prof. J. Tuchandler for fruitful comments.

References

1 M. M. Thackeray, W. I. F. David, P. G. Bruce and J. B. Goodenough, *Mater. Res. Bull.*, 1983, **18**, 461.
2 M. M. Thackeray, P. J. Johnson, L. A. D. Picciotto, P. G. Bruce and J. B. Goodenough, *Mater. Res. Bull.*, 1984, **19**, 179.
3 J. M. Tarascon and D. Guyomard, *J. Electrochem. Soc.*, 1991, **138**, 2864.
4 D. Guyomard and J. M. Tarascon, *J. Electrochem. Soc.*, 1992, **139**, 937.
5 T. Ohzuku, M. Kitagawa and T. Hirai, *J. Electrochem. Soc.*, 1990, **137**, 769.
6 R. J. Gummow, A. de Kock and M. M. Thackeray, *Solid State Ionics*, 1994, **69**, 59.
7 G. Pistoia, A. Antonini, R. Rosati and C. Bellitto, *J. Electrochem. Chem.*, 1996, **410**, 115.
8 K. Amine, H. Tukamoto, H. Yasuda and Y. Fujita, *J. Electrochem. Soc.*, 1996, **143**, 1607.
9 D. Song, H. Ikuta, T. Uchida and M. Wakihara, *Solid State Ionics*, 1999, **117**, 151.
10 Q. Zhong, A. Bonakdarpour, M. Zhang, Y. Gao and J. R. Dahn, *J. Electrochem. Soc.*, 1997, **144**, 205.
11 N. Hayashi, H. Ikuta and M. Wakihara, *J. Electrochem. Soc.*, 1999, **146**, 1351.
12 F. L. Cras, D. Bloch, M. Anne and P. Strobel, *Solid State Ionics*, 1996, **89**, 203.
13 L. Guohua, H. Ikuta, T. Uchida and M. Wakihara, *J. Electrochem. Soc.*, 1996, **143**, 178.
14 S. Bach, M. Henry, N. Baffier and J. Livage, *J. Solid State Chem.*, 1990, **88**, 325.
15 J. P. Pereira-Ramos, *J. Power Sources*, 1995, **54**, 120.
16 P. Barboux, J. M. Tarascon and F. K. Shokoohi, *J. Solid State Chem.*, 1991, **94**, 185.
17 W. Liu, G. C. Farrington, F. Chaput and B. Dunn, *J. Electrochem. Soc.*, 1993, **143**, 879.
18 M. S. Whittingam, *Solid State Ionics*, 1996, **86–88**, 1.
19 S. R. S. Prabaharan, M. S. Michael, T. Premkumar, A. Mani, K. Athinarayanaswamy and R. Gangadharan, *J. Mater. Chem.*, 1995, **5**, 1035.
20 S. R. S. Prabaharan, M. S. Michael, S. Radhakrishna and C. Julien, *J. Mater. Chem.*, 1997, **7**, 1791.
21 M. M. Thackeray, M. F. Mansuetto, D. W. Dees and D. R. Vissers, *Mater. Res. Bull.*, 1996, **31**, 133.
22 C. Julien, *Ionics*, 2000, **6**, 30.
23 C. Julien, L. El-Farh, S. Rangan and M. Massot, *J. Sol–Gel Sci. Technol.*, 1999, **15**, 63.
24 R. D. Shannon, *Acta Crystallogr., Sect. A*, 1976, **32**, 751.
25 C. Julien and G. A. Nazri, *Mater. Res. Soc. Symp. Proc.*, 1999, **548**, 79.
26 C. Julien, A. Rougier, E. Haro-Poniatowski and G. A. Nazri, *Mol. Cryst. Liq. Cryst.*, 1998, **311**, 81.
27 C. Julien, in *Materials for Lithium-Ion Batteries*, ed. C. Julien and Z. Stoynov, NATO-ASI Series, vol. 3–85, Kluwer Academic Publishers, Dordrecht, 2000, p. 309.
28 G. C. Allen and M. Paul, *Appl. Spectrosc.*, 1995, **49**, 451.
29 G. Pistoia, D. Zane and Y. Zhang, *J. Electrochem. Soc.*, 1995, **142**, 2551.
30 J. B. Goodenough, A. Manthiran and B. Wnetrzewski, *J. Power Sources*, 1993, **43–44**, 269.
31 I. G. Austin and N. F. Mott, *Adv. Phys.*, 1969, **18**, 41.
32 A. Yamada and M. Tanaka, *Mater. Res. Bull.*, 1995, **30**, 715.
33 A. Yamada, *J. Solid State Chem.*, 1996, **122**, 160.
34 S. Mukerjee, T. R. Thurston, N. M. Jisrawi, X. Q. Yang, J. McBreen, M. L. Daroux and X. K. Xing, *J. Electrochem. Soc.*, 1998, **145**, 466.
35 X. Q. Yang, X. Sun, S. J. Lee, J. McBreen, S. Mukerjee, M. L. Daroux and X. K. Xing, *Electrochem. Solid State Lett.*, 1999, **2**, 157.